Effects of Dielectric Tube Shape and Pin-Electrode Diameter on the Plasma Plume in Atmospheric Pressure Helium Plasma Jets

Hae Ra Kang, Tae Hun Chung, Hea Min Joh, and Sun Ja Kim

***Abstract*— This paper explores the effects of tube shape and pin electrode diameter on the plume generation and electrical characteristics in atmospheric pressure helium plasma jets generated from a centered-pin electrode inside a dielectric tube. The quartz-covered (or bare) pin electrode and different shapes of the dielectric tube (straight cylinder or conical shape) are employed and their effects are investigated. Optical emission spectra are obtained at different positions along the coaxial direction to determine the axial distributions of the electron excitation temperature for the straight cylinder and conical jets. The rotational temperatures for the both jets are also compared.**

***Index Terms*— Atmospheric pressure plasma jet (APPJ), dielectric tube, pin electrode.**

I. Introduction

ATMOSPHERIC pressure nonthermal plasmas have become great issues of plasma research due to their immense potentials for material processing and biomedical applications [1]. In particular, atmospheric pressure plasma jets (APPJs) can produce local nonthermal plasma, characterized by flexibility, compactness, directionality, and efficiency. Since APPJs generate plasma plumes (PLs) in open space surrounding air rather than in confined discharge gaps, they can be used for direct treatment and there are no limitations on the sizes of the objects to be treated. Atmospheric pressure cold plasma jets represent a rapidly developing technology of great application promise.

A variety of configurations have been proposed for APPJs. Among them, most frequently used APPJs utilize barrier discharges in flows of noble gases in thin dielectric tubes and injected into ambient air. Two main electrode configurations have been considered; with a centered pin electrode inside the tube [2]–[4], and with one or two ring electrodes wrapped around the tube [5]–[11]. The hybrid electrode structure consists of a central (pin or capillary) electrode enclosed within a dielectric tube with a concentric ring electrode wrapped around the tube near the tube nozzle [12]–[16]. The former is sometimes referred to as the cross-field device as its electric field and its flow field are perpendicular to each other [4]. Although the ring type jets are preferred in RF operation [4], [5], the employment of pin electrodes is usually favorable to produce a stronger electric field at moderate applied voltages [4]. A small diameter of the pin electrode with a sharp edge allows for a local enhancement of the electric field and thus a considerable reduction of the breakdown voltage requirement. With a large local curvature of the pin point, the generated electric field is sufficiently high to induce the breakdown and to sustain the resulting plasma at relatively moderate applied voltage.

Physically, the breakdown mechanism of APPJs depends strongly on electron multiplication, which controls the transition from Townsend breakdown to streamer breakdown [17], [18]. When operating at lower frequencies, the plasma jet was found to be constituted of discrete plasma bullets moving at a velocity much higher than the gas velocity. As the plasma bullet travels to further distances, it leaves behind a channel consisting of short-lived and long-lived species. In this regard, the gas flow dynamics within the quartz tube is important for the plasma generation and reactive species transport. The inner diameter of the dielectric tube ranges from about 4–6 mm [4], [6], [7], [12]–[16] to 1–3 mm [5], [8], [9], [19], and down to less than 1 mm [10], [11] depending on applications. PLs generated from small-diameter tubes (typically, less than 3 mm) are usually very slim and not useful for many applications. Therefore, it would be desirable to extend the PL scale by employing medium-diameter discharge tubes (typically, larger than 3 mm). For biomedical applications, APPJs should produce and transport abundant reactive species near room temperature and remotely treat targets minimizing electric shock, current-induced heating, and arcing. Efficient transport of reactive species is expedited when the PL touches the target. Therefore, the control of plume length is important. Of course, the driving power source is one of the important parameters which could significantly affect the characteristics of plasma jets. In this paper, however, our attention is focused on the effects of the geometry of the electrode and dielectric tube on the PL characteristics.

This paper complements and extends our previous study [20]. In this paper, the effects of tube shape (straight cylinder and conical shape) and pin electrode diameter on the plasma characteristics including the plume formation are investigated in atmospheric pressure helium plasma jets generated from a pin electrode inside a dielectric tube. The effect of quartz-covered pin electrode is also investigated.

Manuscript received July 6, 2016; accepted February 23, 2017. Date of publication March 27, 2017; date of current version April 10, 2017. This work was supported by the research fund of Dong-A University. *(Corresponding author: Tae Hun Chung.)*

The authors are with the Department of Physics, Dong-A University, Busan 49315, South Korea (e-mail: thchung@dau.ac.kr).

Color versions of one or more of the figures in this paper are available online at http://ieeexplore.ieee.org.

Digital Object Identifier 10.1109/TPS.2017.2678527

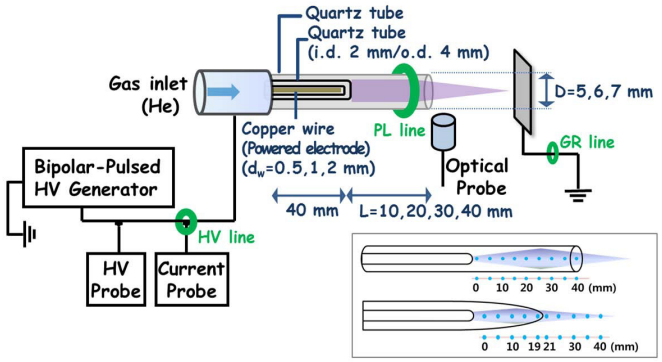

Fig. 1. Schematic of the experimental setup. Two kinds of discharge tubes, a straight cylinder tube or a conical tube, are utilized.

II. Experiments

Fig. 1 depicts the experimental setup and the configuration of the plasma jet investigated in this paper. The plasma jet device consists of a dielectric (quartz) confinement tube (straight cylinder or conical shape) and a centered quartz-covered (or bare) pin electrode which is made up of copper wire with a diameter (d_w) of 0.5, 1, and 2 mm. This device was designed with some modifications to the plasma jet introduced by Lu *et al.* [13]. Quartz discharge tubes (inner diameters $D = 5$, 6, and 7 mm, and outer diameters 7, 8, and 9 mm, respectively) served as the dielectric barrier layer. Without the ring electrode, the dielectric tube only plays the role of guiding the gas flow. The centered pin electrode can either be bare or quartz-covered with a closed right-end. High purity helium (99.997%) was used as the working gas. The distance (L) between the tip of the pin electrode and the nozzle of the dielectric tube can be adjusted from 10 to 40 mm. The sketches of a straight cylinder tube jet and a conical tube jet are illustrated in Fig. 1, respectively.

The plasma was generated by a pulsed bipolar source with a repetition frequency of several tens of kilohertz (EESYS APPS020). A typical operation condition of the plasma jet had an applied voltage of 2.5 kV_{rms} (root-mean-square value), repetition frequency of 50 kHz, and pulsewidth of 5.5 μs. The waveforms of the voltage and the current were measured using a real time digital oscilloscope (LeCroy WS44XS-A) via high-voltage probe (Tektronix P5100) and current probe (Pearson 3972). Three different positions of the current monitor were used in independent experiments (Fig. 1), in order to gain information on the current flowing on all pathways of the equivalent electrical circuit: the high-voltage electrode (HV) line, the PL line, and the ground electrode (GR) line.

To identify reactive species generated in the discharge and subsequently expelled with the gas flow, optical spectra were recorded for emission in the range of 200–900 nm. The emission was collected perpendicular to the plume's propagating direction at several measurement points (z) along the axis of the jets. The light emitted by the plasma was focused by means of optical fiber into the entrance slit of a 0.75 m monochromator (SPEX 1702), equipped with a grating of 1200 grooves per millimeter and slit width of 100 μm. A photosensor amplifier (Hamamatsu C6386-01) was used to observe the wavelength-integrated plasma emission

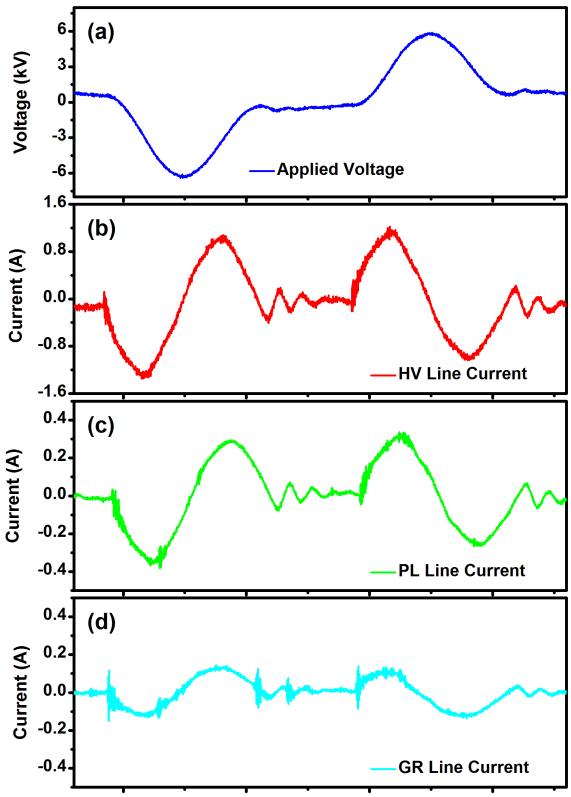

Fig. 2. Waveforms of (a) applied voltages and the total current (b) at HV line, (c) at the PL line, and (d) at GR line for the straight cylinder tube jets driven by a pulsed bipolar source at 50 kHz.

III. Results and Discussion

A. Electrical Characteristics

Fig. 2 shows the waveforms of the applied voltage and the temporal evolutions of the current of HV line, PL line, and GR line for the straight cylinder tube jet operating at a frequency of 50 kHz. The gas flow rate was kept constant at 1 L/min. The voltage across the gas gap (V_g) is simply the difference between the applied voltage (V_a) and the voltage across the dielectric (V_d). Note that V_d follows temporally V_a with a time lag (due to the charges from the plasma volume being collected on the surface of the dielectric), and the temporal profile of the total current resembles that of V_g as shown in Fig. 2(b)–(d) [20]. During the rising slope of the positive applied voltage, discrete current impulses are observed, where sharp peaks are superimposed on the displacement current generated due to capacitances. It was observed that the discharge produced at least two plasma bullets every cycle of the applied voltage, and that the main optical emission occurred at the rising edge of the positive half cycle of the voltage waveform, and that weak light emission signal occurred at the falling edge of the negative half cycle. The optical intensity measured at the electrode tip was found to be nearly in phase with the discharge current [20].

Fig. 3 illustrates the total currents as a function of the applied voltage. As the applied voltage was increased

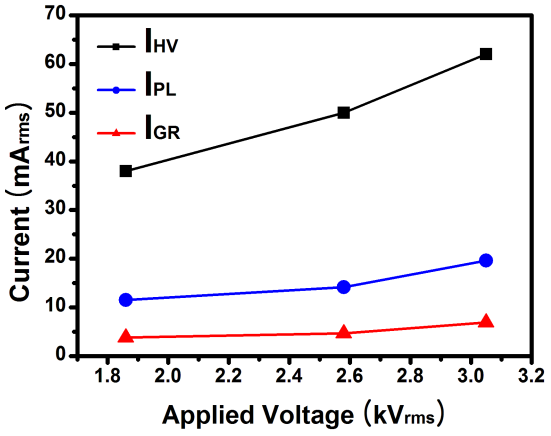

Fig. 3. Total currents (HV line current, PL line current, and GR line current) versus the applied voltage.

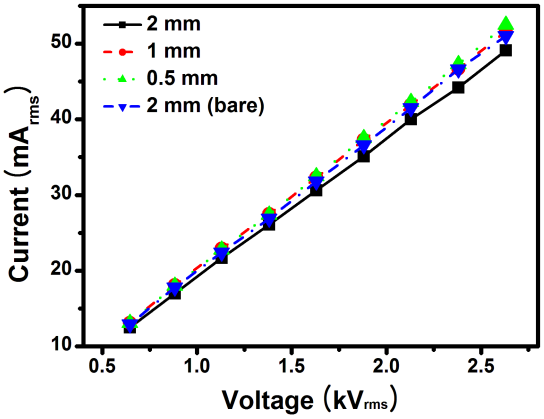

Fig. 4. Current–voltage curves for the straight cylinder plasma jets operated with three different diameters ($d_w = 0.5$, 1, and 2 mm).

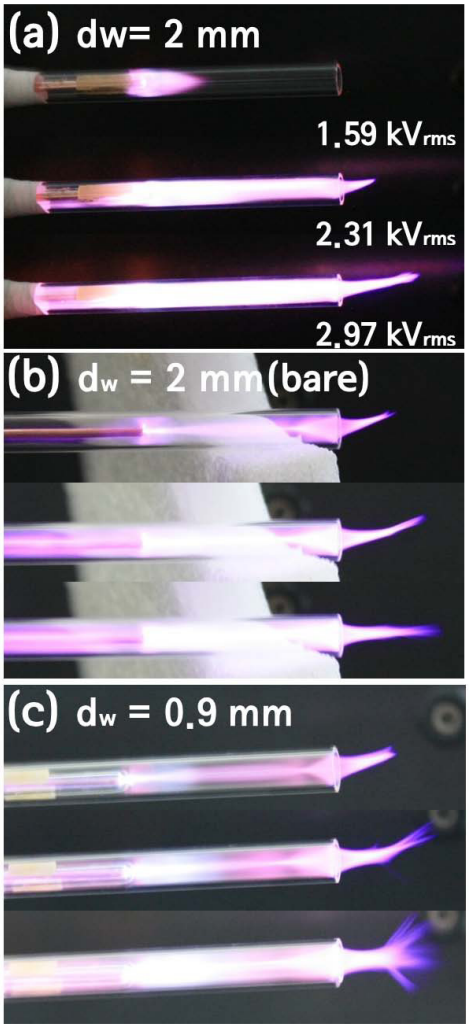

Fig. 5. Photograph of plume in the straight cylinder jet ($D = 5$ mm and $L = 4$ cm) as a function of the applied voltage for three different pin electrodes. (a) $d_w = 2$ mm (quartz-covered pin). (b) $d_w = 2$ mm (bare pin). (c) $d_w = 0.9$ mm (quartz-covered pin).

from 1.86 to 3.05 kVrms, the total currents were increased; from 38 to 62 mArms for the HV line current, from 11.5 to 19.6 mArms for the PL line current, and from 1.86 to 6.91 mArms for the GR line current. It is found that a relatively small portion of the current (5%–10%) is extending out of the discharge tube, flowing along the plasma jet, and then being collected by the GR. The total current consists of three parts such as $I_{\text{tot}} = I_c + I_d + I_p$, where I_c is the conduction current in the pin electrode, I_d is the displacement current, and I_p is the plasma current associated with the ignited plasma. In the PL line current, there is a considerable reduction in I_c. Additional reductions in both I_d and I_p occur in the GR line current.

Fig. 4 shows current–voltage curves for the straight cylinder plasma jets operated with three different diameters ($d_w = 0.5$, 1, and 2 mm) of the quartz-covered pin and with the bare pin ($d_w = 2$ mm). The applied voltage was in the range of 0.6–2.6 kVrms and the measured total current (HV line) was 13–55 mArms. It was observed that the case of 0.5 mm diameter pin had a larger total current. Utilizing the capacitance of a coaxial cable, the equivalent capacitance of the gas gap and the quartz-covered pin electrode can be estimated as

$$C_g = \frac{2\pi\varepsilon_0 l}{\ln\left(\frac{b}{c}\right) + \frac{1}{K}\ln\left(\frac{c}{a}\right)} \tag{1}$$

where l is the length of the pin electrode; a, b, and c are radii of the pin electrode, inner quartz tube (covering the pin), and outer discharge tube, respectively; and K is the dielectric constant of the inner quartz tube. When the inner quartz tube is removed (i.e., in the case of the bare pin electrode, $c \rightarrow a$ and $K \rightarrow 1$), the C_g is reduced to $C_{g0} = (2\pi\varepsilon_0 l/\ln((b/a)))$. The displacement current is written as $I_d = C_g(dV(t)/dt)$. The plasma resistance can be described as $R_p = (\ln(b/c)/2\pi\sigma l)$, where $\sigma = (n_e e^2/m\nu_m)$ is the plasma conductivity. (n_e, e, m are the number density, charge, and mass of electrons, respectively, and ν_m is the electron collision frequency.) Then the plasma current is approximated as $I_p = (V(t)/R_p)$.

With an increase in d_w, the I_c increases slightly because of the reduction of the pin wire resistance due to the increased

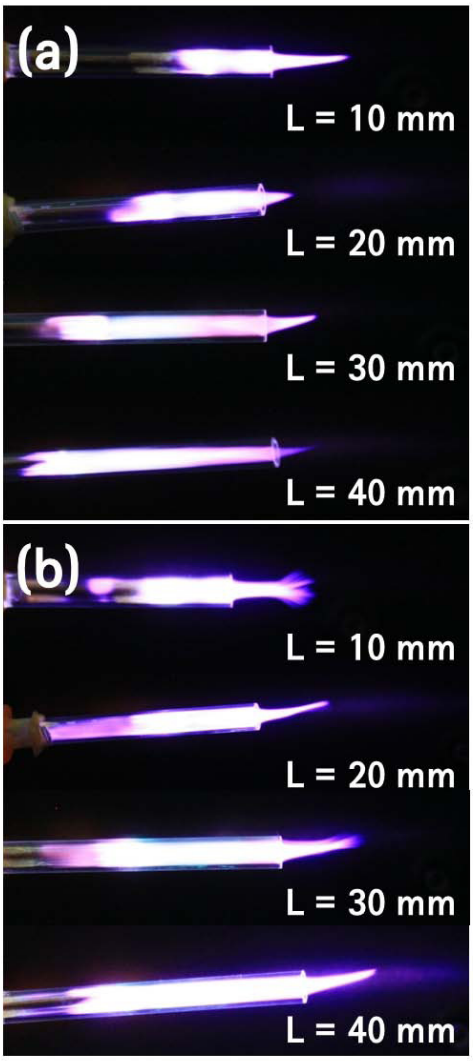

Fig. 6. Photograph of plume in the straight cylinder jet ($D = 5$ mm) as a function of L for two different applied voltages: (a) 1.83 kVrms and (b) 2.54 kVrms.

cross section of the pin. The I_d also increases because C_g is also increased with d_w (or a). However, the plasma current I_p decreases because the plasma resistance R_p is increased due to the reduced plasma density (caused by the decreased electric field). Thus, the change of I_t with the d_w results from the combination of these three parts. It was observed that the case of 0.5-mm diameter pin had a larger total current whereas it had a longer plume. In the case of the 2-mm diameter pin, I_c and I_d are increased, but I_p decreases being dominantly, leading to a reduction in I_{tot}. However, in the case of 1-mm diameter pin, the total current is a little less than that of 0.5-mm pin. For the 2-mm bare pin, the increased plasma density due to enhanced electric field leads to the increase in the plasma current. As a result, in spite of a slight decrease in I_c, the total current increases.

Fig. 5 displays the PL of the straight cylinder jet as functions of applied voltage for different diameters of the pin electrode; (a) 2 mm (quartz-covered pin), (b) 2 mm (bare pin), and (c) 0.9 mm (quartz-covered pin). At applied voltages below 2 kVrms, the jet with a 0.9-mm diameter pin had a

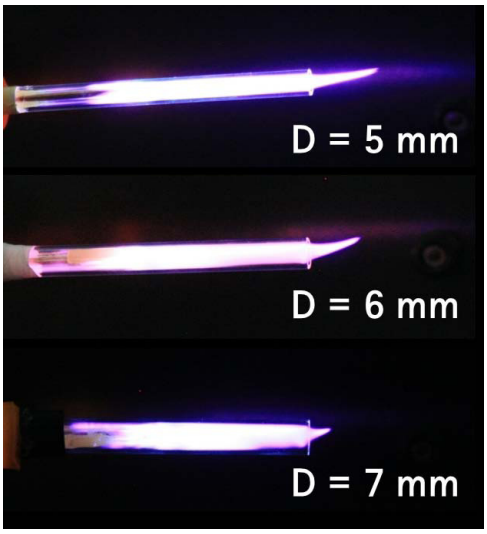

Fig. 7. Photograph of plume in the straight cylinder jet ($L = 4$ cm) as a function of D at the applied voltage of 2.54 kVrms.

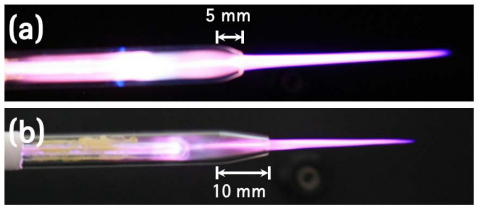

Fig. 8. Photograph of plume in the conical tube jets: the tapering begins at (a) 5 mm and (b) 10 mm from the tube exit.

longer PL. In the case of (c), as the applied voltage increased, the jet front became unstable and filament-like. The instability and filament-like pattern may be related to the gas flow. Plasma generation can also strongly influence the gas flow at the plasma jet outlet [19], [21]. Laminar mode is formed at low gas flow rates, while turbulent mode is produced at higher gas flow rates. The transition from laminar to turbulent mode is closely associated with a noticeable decrease of plasma jet length [22]. The transition from laminar to turbulent mode can be detected by Reynolds number (R_e) defined as

$$R_e = \frac{\rho V D}{\mu} \tag{2}$$

where ρ is the helium density, μ is the viscosity, V is the gas flow velocity, and D is the nozzle diameter. For a typical operation condition (the gas flow rate of 2 L/min and nozzle diameter 5 mm), R_e is about 740. For a fixed gas flow rate, the gas flow velocity is inversely proportional to the square of tube diameter, thus, $VD \propto {}^{1}/_{D}$, which indicates that an increase of tube diameter results in decrease of R_e. However, the ignited plasma can influence the flow transition from laminar to turbulent, while R_e is still far below 2000.

When higher voltages are applied, filamentous pattern was seen in the far postdischarge region, in which many individual discharge channels were formed [see at 2.97 kVrms in Fig. 5(c)]. This tendency was strong for thinner pin electrodes and for bare pin electrodes. This may be related to the electrical coupling between the streamer tip and the

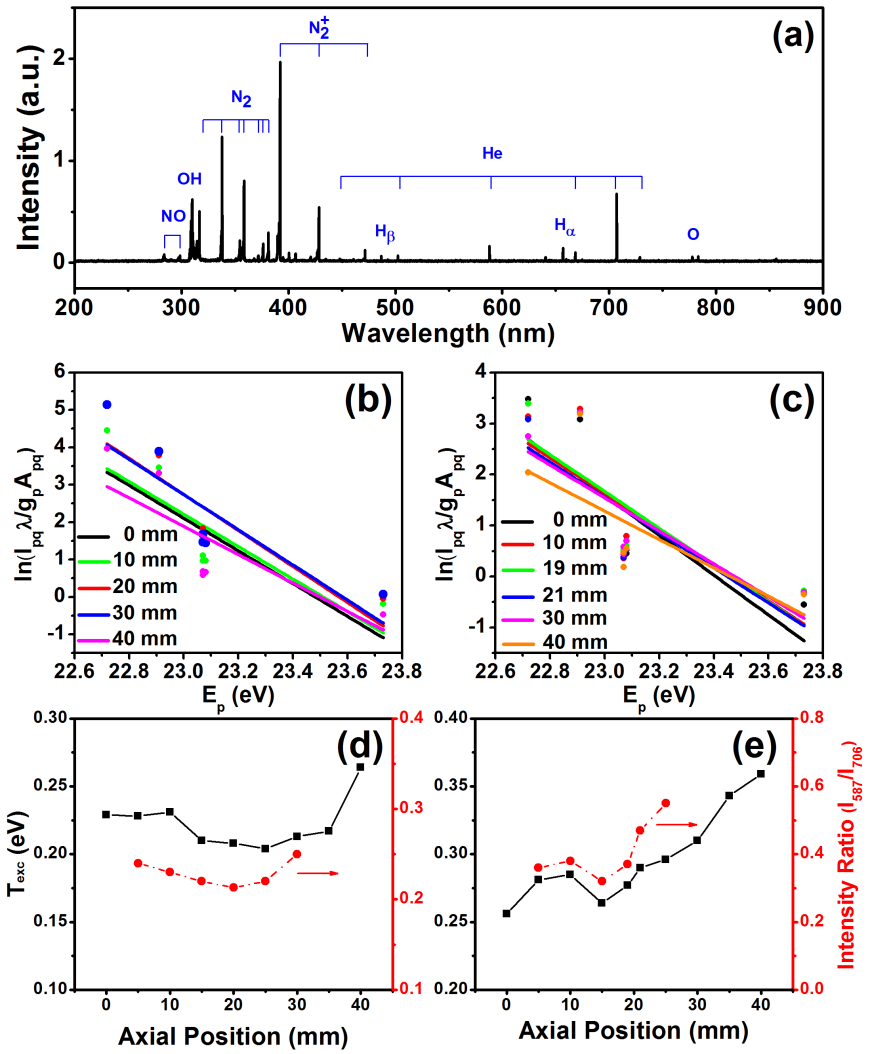

Fig. 9. (a) Optical emission spectra for the straight cylinder tube jet. A Boltzmann plot method was used to estimate the excitation temperature for (b) straight cylinder jet and (c) conical tube jet. Axial distributions of the excitation temperature for (d) straight cylinder jet and (e) conical tube jet.

discharge electrode [23]. The central electrode potential is transferred along the discharge channel to the streamer tip without significant voltage drop. The filamentous pattern in the far postdischarge region was seen only in the straight cylinder jets, not in the conical tube jets. The streamer propagates only in the region of high helium concentration. The shape of the visible filament-like plasma (with narrow branching channels) may be formed by the air diffusion effect. The straight cylinder tube has a larger gas mixing on the radial boundary near the tube exit.

Fig. 6 shows the influence of the distance (L) between the tip of the pin electrode and the tube exit on the plume generation. At the applied voltage of 1.83 kVrms, the case of $L = 10$ mm cm has more intense and longer PLs [Fig. 6(a)]. This may be due to the increased losses of electrons and He metastables by diffusion to the tube wall with increasing L. However, the distance (L) did not make a significant difference in I–V curve for the range of 10–40 mm (figures not shown). At the applied voltage of 2.54 kVrms, the case of $L = 10$ mm exhibits a filamentous pattern in the plume, and the plumes remain stable for all cases of $L = 20$–40 mm [Fig. 6(b)]. This implies that the losses of electrons and He metastables by diffusion to the tube wall do not change much within the range of L 10–40 mm at a higher applied voltages.

It is generally known that smaller tube radii lead to much higher streamer speeds and plasma densities [24]. When the tube radius is 2 mm and above, the plasma propagates primarily along the He–air mixing layer with very little plasma generated on the axis [24]. In this case the discharge is quite similar to a surface ionization wave. This was confirmed by the bullet shape in front view in our previous study [12]. In the tube diameters of the range of 5–7 mm, the internal diameter of the tube (D) was also influential in forming the plume and expelling it from the nozzle. The effect of tube diameter is exhibited in Fig. 7. The case of $D = 5$ mm demonstrates better plasma shape being effective in the plume generation for the straight cylinder tube. In small-diameter tube below 1 mm, the diffusion loss to the wall becomes much larger at decreased tube diameters [25]. However, in the case of large-diameter tube, the trend becomes the opposite. With the increase of tube diameter, the electric field strength in the head of the ionization front caused by the space charge decreases [11].

Fig. 8 compares the PL in conical tube jets (nozzle diameter 3 mm) at 2.31 kVrms and 4 L/min in which the tapering begins at (a) 5 mm and (b) 10 mm from the tube exit. In the conical tube jets, a PL extended up to more than 6 cm from the exit nozzle in the stable stage. A steeply tapered tube jet (a) was observed to have a longer plume than a smoothly tapered tube jet (b). In the steeply tapered tube, the vortex structure of the helium flow became dominant and provided a longer gas residence time, enabling increased plasma activation. The plasma density was then enhanced, which led to the increase in the PL length.

B. Optical Characteristics

The optical emission is collected perpendicular to the plume's propagating direction, and the distribution of emission intensities was obtained at different positions along the axial direction of the jets (for both the straight cylinder and the conical tube jet). The spectrum shows that there are strong nitrogen molecular lines as well as a few helium and oxygen atomic lines. Oxygen and nitrogen species arise because the plasma is ejected into the air where its energetic electrons and He metastables ionize and excite air molecules. The spectra obtained at $z = 15$ mm inside the straight cylinder tube [Fig. 9(a)] reveal that a predominance of N_2^+ line at 391 nm ($B^2\sum_u^+ \rightarrow X^2\sum_g^+$) and N_2^* line at 337.1 nm ($C^3\Pi_u \rightarrow B^3\Pi_g$) followed by the He 706.5-nm line. The lines of the first negative system of N_2^+ at 391, 427, and 471 nm ($B^2\sum_u^+ \rightarrow X^2\sum_g^+$) are attributed to Penning ionization ($He^* + N_2 \rightarrow He + N_2^+ + e^-$) and charge transfer ($He^+ + N_2 \rightarrow He + N_2^+$) followed by direct electron-impact excitation ($e^- + N_2^+ \rightarrow N_2^{+*} + e^-$) [26]. The lines 315, 337, 357, and 380 nm represent the second positive system of nitrogen molecule. The emission spectrum clearly indicates that O (777 nm), OH (309 nm), and NO (283 nm) exist in the PL. In the discharge area, the electron impact dissociation of N_2 and O_2 molecules leads to the formation of atomic oxygen and the breaking of the strong bond in the N_2 molecule by vibrational excitation and dissociation. Atomic oxygen may also be generated though Penning dissociation ($N_2^* + O_2 \rightarrow N_2 + O + O$). The OH radicals are produced from water vapor in the helium flow, which is humidified by water adsorbed on the inner surface of the helium line and the discharge tube. The presence of nitric oxide (NO) at 283 nm is due to the chemical conversion of N and O_2 (or N and O) [27]. The emission lines at 656 and 486 nm correspond to the H_α line and H_β, respectively, which are generated by the collision between water vapor molecule and electrons ($H_2O + e \rightarrow H + OH + e$). These highly reactive species such as O, OH, and NO are considered to be the most effective agents in attacking cells or organic material in general.

The electron excitation temperature is estimated by using a Boltzmann plot method applied to several excited helium emission lines (447, 501, 587, 667, 706, and 728 nm) [9], [25]. From the measurement of intensity and wavelength, a Boltzmann plot is obtained for the helium plasma, and the electron excitation temperature (T_{exc}) can be estimated.

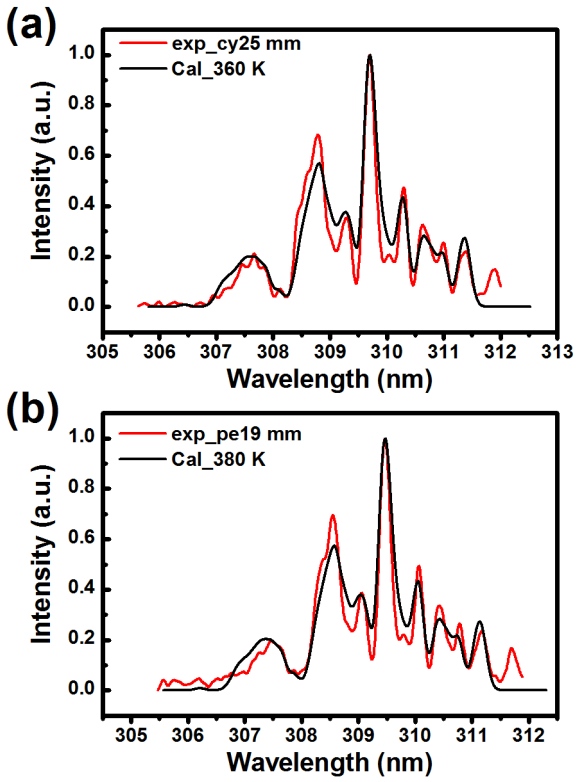

Fig. 10. Measured and simulated optical emission spectra around the OH line at 309.6 nm to determine the rotational temperature for (a) straight cylinder jet and (b) conical tube jet.

The electron excitation temperature estimated by Boltzmann plot method is known to be an order of magnitude lower than the expected values of electron temperature in helium plasmas [25]. Fig. 9(b) and (c) presents Boltzmann plots to calculate the electron excitation temperature for the straight tube jet and the conical tube jet, respectively. The calculated T_{exc} of the conical tube jet is found to be in the range of 0.25–0.30 eV, whereas T_{exc} of the straight tube jet is in the range of 0.2–0.25 eV. This difference is attributable to an effective increase of the air mixing in straight tube, thus resulting in an increase in the electron-neutral collision frequency. As the excitation temperature may be used as a rough indication of the electron temperature [4], these results suggest that the conical tube jet can achieve higher mean electron energy. Fig. 9(d) and (e) represents the axial variation of the electron excitation temperature for the straight tube jet and the conical tube jet, respectively. The electron excitation temperature decreases slightly toward the outlet inside the quartz tube and then begins to rise near the tube outlet [9]. This phenomenon might also be ascribed to the increase of the air mixing with being close to the tube exit. The intensity ratio of two atomic lines, 587 nm ($3d\ ^3D \rightarrow 2p^3P$) and 706 nm ($3s\ ^3S \rightarrow 2p\ ^3P$), is equivalent to the ratio of upper state's density, which depends on the electric field or the electron energy [18]. The intensity ratio varies axially in a similar fashion to that of the excitation temperature. The increases in T_{exc} and the intensity ratio outside the conical tube imply the generation of a higher fraction of high-energy electrons not only in the discharge (where the electron energy distribution

is directly related to the applied electric field), but also in the plasma bullets produced outside the tube [18].

The plasma (gas) temperature (T_g) can be deduced from the rotational temperature (T_r) of diatomic species, which is expected to be in equilibrium with T_g for atmospheric pressure plasmas. The rotational temperature of a molecule can be obtained by comparing the synthetic diatomic molecular spectrum with measured one [28]. To obtain the best fit between the experimental and the synthetic spectral bands, a least-square procedure is used. The fine structure of the rotational band of OH ($A\ ^2\sum^+ \rightarrow X^2\Pi$ transition) from 306 nm to 310 nm is fit to obtain the gas temperature. A typical fitting of the measured band spectrum with the synthetic spectrum is shown in Fig. 10. The simulated spectrum at $T_r = 380$ K gives the best fit to the experimental spectrum. Although the values of T_r for the straight cylinder and conical tube jets have some difference, but they lie within the level of uncertainty associated with fitting procedure [25].

IV. Conclusion

Atmospheric pressure helium plasma jets generated from a centered-pin electrode inside a dielectric tube are studied to determine optimal operational conditions for biomedical applications. We compared the plume characteristics for the bare pin electrode and quartz-covered pin electrode. We investigated the effects of pin diameter, dielectric tube diameter, and the shape of the tube (straight cylinder and conical) on the plume generation and electrical characteristics. The plume length and the plume luminosity exhibited quite a strong dependence on the configurations of electrode and dielectric tube. It was observed as follows.

1) The plasma jets with thinner diameter pin electrode had a brighter and longer plume.
2) The plasma jet with the bare pin electrode had a brighter and longer plume than the jet with the quartz-covered pin electrode.
3) The plume length increased with a decrease in the tube diameter in straight cylinder jet, but it needs an optimized nozzle size in the conical tube jet.
4) Conical tube jets have higher electron excitation temperature than that of the straight cylinder tube jets.

The rotational temperatures for the both jets are almost comparable.

References

[1] M. Laroussi and T. Akan, "Arc-free atmospheric pressure plasma jets: Areview," *Plasma Process. Polym.*, vol. 4, no. 9, p. 777, Nov. 2007.

[2] Q. Xiong *et al.*, "Temporal and spatial resolved optical emission behaviors of a coldatmospheric pressure plasma jet," *J. Appl. Phys.*, vol. 106, no. 8, p. 083302, Oct. 2009.

[3] X. Lu, M. Laroussi, and V. Puech, "On atmospheric-pressure non-equilibriumplasma jets and plasma bullets," *Plasma Sour. Sci. Technol.*, vol. 21, no. 3, p. 034005, May 2012.

[4] J. L. G. Walshand and M Kong, "Contrasting characteristics of linear-field and cross-field atmosphericplasma jets," *Appl. Phys. Lett.*, vol. 93, no. 11, p. 111501, Sep. 2008.

[5] J. L. Walsh, F. Iza, N. B. Janson, V. J. Law, and G. M. Kong, "Three distinctmodes in a cold atmospheric pressure plasma jet," *J. Phys. D, Appl. Phys.*, vol. 43, no. 7, p. 075201, Feb. 2010.

[6] A. V. Nastuta, V. Pohoata, and I. Topala, "Atmospheric pressure plasma jet-Living tissue interface: Electrical, optical, and spectral characterization," *J. Appl. Phys.*, vol. 113, p. 183302, May 2013.

[7] R. Ye and W. Zheng, "Temporal-spatial-resolved spectroscopic study on the formation of an atmospheric pressure microplasma jet," *Appl. Phys. Lett.*, vol. 93, no. 7, p. 071502, Jul. 2008.

[8] E. Karakas, M. A. Akman, and M. Laroussi, "The evolution of atmospheric-pressurelow-temperature plasma jets: Jet currentmeasurements," *Plasma Sour. Sci. Technol.*, vol. 21, no. 3, p. 034016, May 2012.

[9] K. Yambe and S. Satou, "Investigation of helium plasma temperature in atmospheric-pressure plasma plume using line pair method," *Phys. Plasmas*, vol. 23, no. 2, p. 023509, Feb. 2016.

[10] I. Topala and M. Nagatsu, "Capillary plasma jet: A low volume plasma source for life science applications," *Appl. Phys. Lett.*, vol. 106, no. 5, p. 054105, Feb. 2015.

[11] R. Talviste, I. Jõgi, J. Raud, and P. Paris, "The effect of dielectric tube diameter on the propagation velocity of ionization waves in a He atmospheric-pressure micro-plasma jet," *J. Phys. D, Appl. Phys.*, vol. 49, p. 195201, Apr. 2016.

[12] H. S. Park, S. J. Kim, H. M. Joh, T. H. Chung, S. H. Bae, and S. H. Leem, "Optical and electrical characterization of an atmospheric pressure microplasma jet with a capillary electrode," *Phys. Plasmas*, vol. 17, p. 033502, Mar. 2010.

[13] X. Lu, Z. Jiang, Q. Xiong, Z. Tang, X. Hu, and Y. Pan, "An 11 cm long atmospheric pressure cold plasma plume for applications of plasma medicine," *Appl. Phys. Lett.*, vol. 92, p. 081502, Feb. 2008.

[14] M. Keidar *et al.*, "Cold atmospheric plasma in cancer therapy," *Phys. Plasmas*, vol. 20, no. 5, p. 057101, 2013.

[15] A. Shashurin, M. Keidar, S. Bronnikov, R. A. Jurjus, and M. A. Stepp, "Living tissue under treatment of cold plasma atmospheric jet," *Appl. Phys. Lett.*, vol. 93, no. 18, p. 181501, 2008.

[16] Q. Xiong, A. Y. Nikiforov, X. P. Lu, and C. Leys, "High-speed dispersed photographing of an open-air argon plasma plume by a grating–ICCD camera system," *J. Phys. D, Appl. Phys.*, vol. 43, no. 41, p. 415201, Aug. 2010.

[17] X. Duan, F. He, and J. Ouyang, "Prediction of atmospheric pressure glow discharge in dielectric-barrier system," *Appl. Phys. Lett*, vol. 96, no. 23, p. 231502, Jun. 2010.

[18] J. Jarrige, M. Laroussi, and E. Karakas, "Formation and dynamics of plasma bullets in a non-thermal plasma jet: Influence of the high-voltage parameters on the plume characteristics," *Plasma Sour. Sci. Technol.*, vol. 19, no. 6, p. 065005, Oct. 2010.

[19] P. K. Papadopoulos *et al.*, "Interpretation of the gas flow field modification induced by guided streamer ('plasma bullet') propagation," *J. Phys. D, Appl. Phys.*, vol. 47, p. 425203, Sep. 2014.

[20] H. M. Joh, H. R. Kang, T. H. Chung, and S. J. Kim, "Electrical and optical characterization of atmospheric-pressure helium plasma jets generated with a pin electrode: Effects of the electrode material, ground ring electrode, and nozzle shape," *IEEE Trans. Plasma Sci.*, vol. 42, no. 12, pp. 3656–3667, Dec. 2014.

[21] X. Pei *et al.*, "Dynamics of the gas flow turbulent front in atmospheric pressure plasma jets," *Plasma Sour. Sci. Technol.*, vol. 25, p. 035013, Apr. 2016.

[22] D. J. Jin, H. S. Uhm, and G. Cho, "Influence of the gas-flow Reynolds number on a plasma column in a glass tube," *Phys. Plasmas*, vol. 20, no. 8, p. 083513, Aug. 2013.

[23] A. Shashurin and M. Keidar, "Experimental approaches for studying non-equilibrium atmosphericplasma jets," *Phys. Plasmas*, vol. 22, p. 122002, Oct. 2015.

[24] X. Lu, G. V. Naidis, M. Laroussi, and K. Ostrikov, "Guided ionization waves: Theory and experiments," *Phys. Rep.*, vol. 540, p. 123, Mar. 2014.

[25] I. Jõgi, R. Talviste, J. Raud, K. Piip, and P. Paris, "The influence of the tube diameter on the properties of an atmospheric pressure He micro-plasma jet," *J. Phys. D, Appl. Phys.*, vol. 47, p. 415202, Sep. 2014.

[26] W.-C. Zhu, Q. Li, X.-M. Zhu, and Y.-K. Pu, "Characteristics of atmospheric pressure plasma jets emerging into ambient air and helium," *J. Phys. D, Appl. Phys.*, vol. 42, no. 20, p. 202002, Sep. 2009.

[27] X. L. Deng, A. Yu, A. Y. Nikiforov, P. Vanraes, and Ch. Leys, "Direct current plasma jet at atmospheric pressure operating in nitrogen and air," *J. Appl. Phys.*, vol. 113, no. 2, p. 023305, Jan. 2013.

[28] S. Y. Moon and W. Choe, "A comparative study of rotational temperatures using diatomic OH, O_2 and $N2^+$ molecular spectra emitted from atmospheric plasmas," *Spectrochimica Acta Part B, Atomic Spectrosc.*, vol. 58, pp. 249–257, Feb. 2003.

Authors' photographs and biographies not available at the time of publication.